Ambipolar Doping of Monolayer FeSe by Interface Engineering

Fang-Jun Cheng(程方君)[1], Yi-Min Zhang(张一民)[1], Jia-Qi Fan(范嘉琪)[1], Can-Li Song(宋灿立)[1,2*], Xu-Cun Ma(马旭村)[1,2], and Qi-Kun Xue(薛其坤)[1,2,3,4]

[1]*State Key Laboratory of Low-Dimensional Quantum Physics, Department of Physics, Tsinghua University, Beijing 100084, China*
[2]*Frontier Science Center for Quantum Information, Beijing 100084, China*
[3]*Beijing Academy of Quantum Information Sciences, Beijing 100193, China*
[4]*Southern University of Science and Technology, Shenzhen 518055, China*

(Received 31 March 2023; accepted manuscript online 26 June 2023)

We report on ambipolar modulation doping of monolayer FeSe epitaxial films grown by molecular beam epitaxy and *in situ* spectroscopic measurements via a cryogenic scanning tunneling microscopy. It is found that hole doping kills superconductivity in monolayer FeSe films on metallic Ir(001) substrates, whereas electron doping from polycrystalline $IrO_2/SrTiO_3$ substrate enhances significantly the superconductivity with an energy gap of 10.3 meV. By exploring substrate-dependent superconductivity, we elucidate the essential impact of substrate work functions on the superconductivity of monolayer FeSe films. Our results therefore offer a valuable reference guide for further enhancement of the transition temperature T_c in FeSe-based superconductors by interface engineering.

DOI: 10.1088/0256-307X/40/8/086801

Superconductivity in monolayer FeSe films grown on $SrTiO_3(001)$ substrates,[1] which was discovered in 2012 and thus far keeps a record for the highest transition temperature (T_c) in iron-based superconductors, has continued to attract attention in the community of high-T_c superconductors. Compared with its bulk counterpart, the superconducting energy gap Δ changes from 2.2 meV to $\sim$20 meV in the monolayer $FeSe/SrTiO_3(001)$ films. The subsequent quest for a mechanistic understanding of this tenfold increase in Δ has led to a variety of surface-sensitive and bulk measurements as well as interfacial engineering of the hybrid structures. For instance, angle-resolved photoemission spectroscopy reported a $T_c \sim 65$ K in monolayer $FeSe/SrTiO_3(001)$,[2] which is consistent with tunneling measurements.[3] Although some *ex situ* transport and diamagnetic measurements present certain varieties of T_c in the range from 40 K to 65 K,[1,3,4] *in situ* transport experiments have revealed signature of T_c up to $\sim$100 K.[5–14] Phenomenally, two major factors, i.e., charge transfer and interface-enhanced electron–phonon (e–ph) coupling, have been suggested to corporately drive the enhancement of superconductivity.

Inspired by this proposal, interfacial engineering has been extensively employed to understand the underlying mechanism of the FeSe-based high-T_c superconductivity and search for higher-T_c superconductors. Along this direction, it has been discovered that interface-enhanced superconductivity likewise exists in monolayer FeSe films supported by the $BaTiO_3$,[15,16] TiO_2,[17,18] and MgO[19] substrates. On the other hand, the influence of alkali-metal electron doping on monolayer and multilayer FeSe films has also been investigated in experiment.[20,21] It was found that through doping of potassium atoms, the pristine non-superconducting bilayer FeSe on $SrTiO_3$ can be driven into the high-T_c superconducting phase and intrinsic multilayer FeSe films can achieve significantly increased superconducting gaps. The results compellingly demonstrate the important role of electron doping on the superconducting properties of monolayer FeSe. However, a complete picture how these hybrid structures prompt the high-T_c superconductivity of monolayer FeSe remains to be explored. In this work, we attempt to realize ambipolar doping of the monolayer FeSe films by growing them on noble metal Ir and its oxide IrO_2 on Nb-doped $SrTiO_3(001)$ substrates, respectively. The results show that hole doping kills the superconductivity of monolayer FeSe on Ir(001) substrate, while monolayer $FeSe/IrO_2$ has a significantly enhanced superconductivity most likely due to the interfacial electron doping. Comparing the work functions of these two substrates as well as those of other systems, we reveals the important role of substrate work functions in driving the superconductivity enhancement of FeSe-derived heterostructures.

Our experiments were conducted on a commercial ultrahigh vacuum (UHV) scanning tunneling microscopy (STM) apparatus (Unisoku), connected to a molecular beam epitaxy (MBE) chamber for *in situ* sample preparation. Nb-doped (0.05 wt%) $SrTiO_3(001)$ substrates were first degassed at 600 ℃, and then annealed at 1200 ℃ for 20 min to obtain flat surface with the well-known 2×2 reconstruction, on which Ir(001) and IrO_2 films were grown by depositing high-purity Ir (99.9%) source from an e-beam evaporator in Se and ozone (1.0×10^{-5} Torr) environments, respectively. Followed by these procedures, we co-deposited Fe (99.995%) and Se (99.9999%) under Se-rich conditions and then annealed them in UHV at 470 ℃ to

*Corresponding author. Email: clsong07@mail.tsinghua.edu.cn
© 2023 Chinese Physical Society and IOP Publishing Ltd

obtain stoichiometric monolayer FeSe as usual. The STM measurements of film morphology and differential conductance spectroscopy (dI/dV) were all performed at 4.2 K with a polycrystalline PtIr tip, which was firstly cleaned by electron beam bombardment in UHV and appropriately conditioned on MBE-grown Ag(111) films. Tunneling spectra were acquired using a standard lock-in technique with a small bias modulation at 981 Hz.

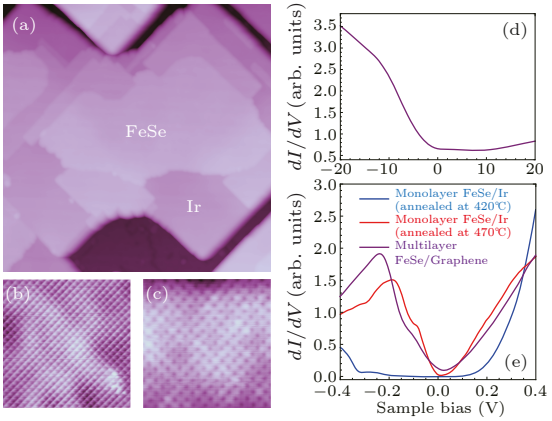

Fig. 1. (a) STM topography (100 nm × 100 nm, V = 3.0 V, I = 30 pA) of a monolayer FeSe film grown on ∼2.8 nm thick Ir island after annealing at 470 ℃. [(b), (c)] Zoom-in STM topographies showing atomically resolved Ir(001) (10 nm × 10 nm, V = 50 mV, I = 120 pA) and FeSe(001) (6 nm × 6 nm, V = 4 mV, I = 150 pA) surfaces, respectively. (d) Low-lying dI/dV spectrum (V = 20 mV, I = 300 pA) on the monolayer FeSe/Ir films upon annealing at 470 ℃ for more than 2 h). (e) Comparison of large-energy-scale dI/dV spectra (V = 0.4 V, I = 300 pA) of monolayer FeSe films on Ir(001) (blue and red curves corresponding to post-annealing at 420 ℃ and 470 ℃, respectively) and multilayer FeSe on epitaxial graphene (purple curve).

Figure 1(a) shows a representative STM topography of the epitaxial Ir(001) films which follow a typical Volmer–Weber growth mode on the $SrTiO_3$(001) substrates, partly covered by the monolayer FeSe films. Note that we can easily obtain single crystalline Ir(001) films by co-depositing Ir and Se sources at a substrate temperature of 600 ℃, with the Se species acting as surfactants. Otherwise, it proves impossible to form large-area Ir islands by solely depositing Ir atoms at various substrate temperatures, consistent with a previous report.[22] Here the monolayer thickness of FeSe film can be readily determined by measuring its topographic height from the uncovered Ir surface, which is approximately 0.57 nm, close to the one-unit-cell thickness of FeSe (0.55 nm). Figures 1(b) and 1(c) illustrate the STM topographies of Ir(001) and FeSe(001) films, respectively. Evidently, the Ir islands show a clear square lattice with an in-plane lattice parameter of $a = b = 3.8$ Å, agreeing nicely with the (001) plane of its face-centered-cubic structure. Such a lattice constant shows a good matching to that of FeSe (3.78 Å), which thus ensures a perfect epitaxy of monolayer FeSe films and minimizes the epitaxial strain, as justified from Fig. 1(c).

Despite perfect epitaxy, monolayer FeSe films show no signature of superconductivity on the metallic Ir films. This has been unambiguously demonstrated by measuring the low-lying electronic density of states (DOS) of the monolayer FeSe and Ir films by STM. As illustrated in Fig. 1(d), the monolayer FeSe films always have a characteristic of smoothly varying DOS around Fermi level E_F, instead any gap opening anticipated for superconductivity. To find the possible cause of the absent superconductivity, we have further acquired large-energy-scale dI/dV spectra of the monolayer FeSe films on Ir(001), as shown in Fig. 1(e). As the post-growth annealing temperature is below 420 ℃, the monolayer FeSe films exhibit a semiconductive behavior due to the Fe vacancies.[23] With further annealing at elevated temperatures, the Fe vacancies can be gradually eliminated and form a highly stoichiometric films. Correspondingly, the monolayer FeSe films change from semiconductor to metal, featured by finite DOS around E_F and a characteristic peak near −0.2 V. This peak should arise from the Fe 3d band[10] and likewise develops in multilayer FeSe films grown on double-layer graphene substrate. However, a careful comparison between them reveals that the peak is obviously shifted towards E_F, indicating hole transfer from Ir to monolayer FeSe films. Note that such shift holds true as well for the DOS kink near −0.1 eV, albeit smaller, and the deviation should derive from the Ir substrate-induced tiny variation of the electronic band structure of the FeSe film. This contrasts markedly with the case of monolayer FeSe films on $SrTiO_3$(001) and TiO_2 where the downward shifting of the similar DOS peak is a hallmark of injection of electrons from the relevant substrates to monolayer FeSe, thereby prompting superconductivity there.[1,17,23]

The distinctly different charge (electron or hole) transfer bears responsibility for the enhanced or quenched superconductivity of monolayer FeSe. To shed more insight into this scenario, we have further prepared monolayer FeSe films on the iridium dioxide (IrO_2), which belongs to a nonsymmorphic crystal and has a rutile-like structure (space group: $P4_2/mnm$) similar to rutile TiO_2. Due to a large lattice mismatch between the rutile IrO_2 ($a = b = 4.505$ Å, $c = 3.158$ Å)[24] and underlying $SrTiO_3$(001) substrates ($a = b = c = 3.905$ Å), polycrystalline IrO_2 films with thickness of ∼1.5 nm routinely grow in a quasi layer-by-layer mode, as revealed in Fig. 2(a). The tunneling dI/dV spectra exhibit a uniform semiconductor-like feature, with E_F closer to the conduction band [see the inserted curve in Fig. 2(a)]. Similar result has also been reported in epitaxial IrO_2 films by pulsed laser deposition.[24] Albeit polycrystalline form, the subsequent growth of FeSe leads to surprisingly flat and single crystalline epitaxial films, as clearly revealed in Figs. 2(b) and 2(c). This resembles those grown on other oxide substrates.[10,23] A more astonishing similarity is a superconducting energy gap that uniquely develops on these oxides-supported monolayer FeSe films [Fig. 2(d)]. The superconducting energy gap is estimated to be approximately 10.3 meV, which appears to be smaller than 20.1 meV in monolayer FeSe/$SrTiO_3$(001) films but appreciably larger than 2.2 meV in bulk FeSe.[25] Without loss of generality, this result hints at appreciable electron transfer from IrO_2 to the monolayer FeSe films,[17] although it

remains to be determined in the future.

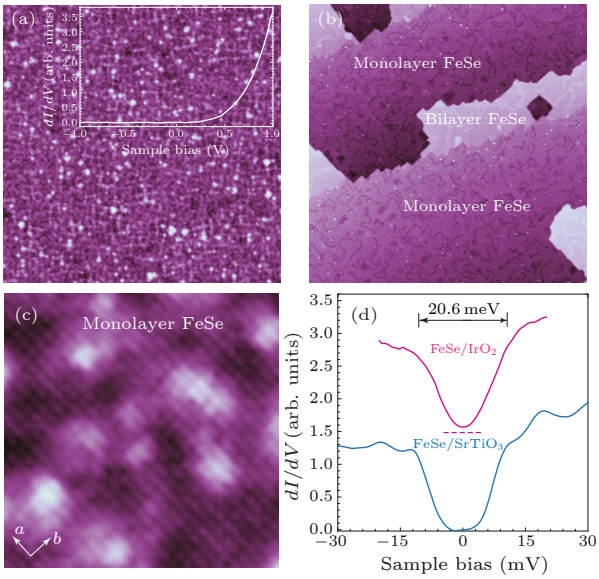

Fig. 2. (a) Typical morphology of polycrystalline IrO_2 films ($50\,\text{nm} \times 50\,\text{nm}$, $V = 0.7\,\text{V}$, $I = 80\,\text{pA}$) on Nb:$SrTiO_3$(001) upon annealing at 750 ℃. Inset: dI/dV spectrum ($V = 1.0\,\text{V}$, $I = 300\,\text{pA}$) showing insulating behavior on polycrystalline IrO_2 film. (b) STM topography ($400\,\text{nm} \times 400\,\text{nm}$, $V = 3.0\,\text{V}$, $I = 30\,\text{pA}$) showing step-flow growth of FeSe thin films on IrO_2 along the terrace of $SrTiO_3$(001). (c) Atomically resolved STM topography ($10\,\text{nm} \times 10\,\text{nm}$, $V = 30\,\text{mV}$, $I = 100\,\text{pA}$) of monolayer FeSe on IrO_2. The a and b axes correspond to either of Se–Se nearest-neighbor directions. (d) Contrast of low-energy dI/dV spectra ($V = 20\,\text{mV}$, $I = 300\,\text{pA}$) of monolayer FeSe on IrO_2 (magenta curve) and $SrTiO_3$ (blue curve). Here, the monolayer FeSe on $SrTiO_3$(001) is grown at 450 ℃ and annealed at 500 ℃. Horizontal dashed line indicates the corresponding position of zero dI/dV value.

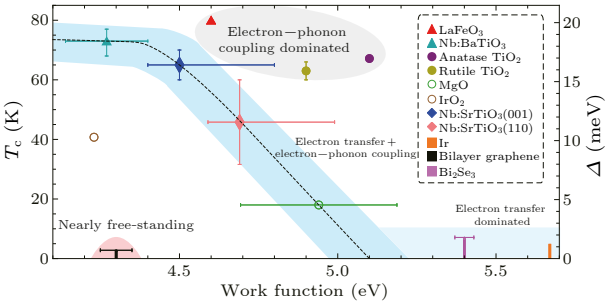

Fig. 3. Substrate-dependent T_c of the monolayer FeSe films and the work functions W of $LaFeO_3$,[26] Nb:$BaTiO_3$(001),[15,16,27] anatase TiO_2(001),[17,28] rutile TiO_2(100),[18,28] MgO(001),[19,29] NC IrO_2 (this work),[30] Nb:$SrTiO_3$(001),[2,10,31,32] Nb:$SrTiO_3$(110),[32–35] Ir(001) (this work),[36] bilayer graphene on 6H-SiC(0001)[37,38] and Bi_2Se_3(0001) substrates.[39,40] The data of monolayer FeSe on Ir, Bi_2Se_3 and bilayer graphene are shown in color bars indicating that their T_c values are not higher than 4.2 K, 6.5 K and 2.2 K, respectively. Relevant discussions are described in the text.

Considering the previous studies primarily on electron-doped FeSe films,[1–21] we have now arrived at the conclusion that the hole and electron dopants kill and enhance superconductivity of monolayer FeSe, respectively. In the following, we show that the distinct charge transfer from Ir and IrO_2 to monolayer FeSe roots at the difference in work functions between Ir and IrO_2. As already measured before, the work functions of Ir(001) and IrO_2 films are 5.67 eV[36] and 4.23 eV,[30] respectively, while the work function of the monolayer FeSe films slightly changes with the post-growth annealing temperature from 4.8 eV to 5.2 eV.[10] In the present case, the monolayer FeSe films were annealed at 470 ℃ and their work function approximates 5.0 eV. Upon brought in close contact, the difference in work functions between the monolayer FeSe and Ir(IrO_2) would cause charge transfer to make the Fermi levels on both sides in alignment. As for the monolayer FeSe/Ir(001) films, the electrons transfer from FeSe to Ir due to the larger work function of Ir, thereby leading to a depletion of electrons, or equivalently hole doping in monolayer FeSe. By contrast, the Fermi level of IrO_2 is higher than that of monolayer FeSe before contact, which causes electron transfer from IrO_2 to monolayer FeSe upon contact. Thus, the T_c of monolayer FeSe is greatly enhanced on IrO_2. It is worth noting that although the Hall experiments show hole-type carriers in IrO_2, they actually do not reflect the total carrier concentration and distribution due to the complex multiband structure of IrO_2. A recent angle-resolved photoemission spectroscopy experiment on IrO_2 films demonstrates that as the film thickness gradually decreases, the energy band of bulk IrO_2 will be quantized along the out-of-plane direction. Additional electron-like bands become apparent and evolve with film thickness.[41] Our scanning tunneling spectroscopy also shows that the Fermi level of the IrO_2 film is closer to the conduction band [see the inset of Fig. 2(a)] similar to the Nb-doped $SrTiO_3$(001), indicating that carriers near the surface of the IrO_2 film are primarily of electrons. They possibly originate from the inevitable oxygen vacancies that lead to a lower work function in IrO_2.[30]

In order to support the above claim, we plot the evolution of T_c in monolayer FeSe with the work functions of eleven different substrates that have been ever used to grow monolayer FeSe films (Fig. 3). Here we reasonably assume that the T_c and superconducting gap Δ of the FeSe films on different substrates satisfy the relationship of $2\Delta/k_BT_c = 5.87$.[18] Based on this formula, we can estimate T_c values of monolayer FeSe films on IrO_2 and anatase TiO_2 substrates from the superconducting energy gap Δ, measured directly in STM and angle-resolved photoemission spectroscopy measurements. It can be immediately seen that the T_c depends crucially on the work functions W of most substrates used. Specifically, the T_c value scales inversely with W for $4.4\,\text{eV} < W < 5.1\,\text{eV}$. As W exceeds 5.0 eV, a value of the work function of monolayer FeSe, the superconductivity disappears owing to the hole doping from the substrates. On the contrary, as the substrate work function W is lower than that that of FeSe, the T_c alters slowly with W. This hints at an optimal doping for the superconductivity and matches fairly with

a recent report in which the T_c is robust against the significantly lowered surface work functions of $LaTiO_3/SrTiO_3$ substrates.[42]

Despite this important finding, there exist some points that somewhat deviate from the whole trend (see the dashed line) due to their respective particularities. For example, the T_c of 1 UC-FeSe/IrO_2 is significantly lower than the expected value. The most possible reason is that the present IrO_2 film is polycrystalline rather than a single crystal, which may lead to appreciable interfacial disorders and is detrimental to long-range electron pairing. On the other hand, the work function at the grain boundary and line defects may increase compared to the bulk state.[43] This will undoubtedly reduce the electron transfer to the monolayer FeSe films to some extent. For the FeSe thin films grown on the bilayer graphene/6H-SiC(0001), although the work function of the substrates is only 4.3 eV,[38] the FeSe films are almost suspended to induce no large change transfer.[37] Therefore, they preserve the intrinsic nature of FeSe superconductors. By contrast, the Δ values of monolayer FeSe/TiO_2 in both rutile and anatase phases are close to that of monolayer FeSe/$SrTiO_3$(001), albeit relatively high work functions.[28] According to the previous theoretical analysis, the interfacial e–ph coupling strength scales inversely with the dielectric constant and the energy of the longitudinal surface modes of the substrates.[5] The dielectric constant of TiO_2 is much smaller than that of $SrTiO_3$,[18] so it is possible that the enhanced T_c of monolayer FeSe/TiO_2 systems is mainly dominated by the interfacial e–ph coupling. This echoes a recent finding of an enormous enhancement of T_c up to 80 K in FeSe/$LaFeO_3$, which has been attributed to the stronger interfacial e–ph coupling than that in FeSe/$SrTiO_3$.[26]

In summary, we have realized the ambipolar doping of monolayer FeSe films by growing them on two totally different substrates Ir and IrO_2, and investigated the role of work function in charge transfer and superconductivity. Although electron doping from IrO_2 can significantly enhances superconductivity of monolayer FeSe, the hole doping from Ir plays the opposite role. We further clarify the underlying doping mechanism as the work function difference between the FeSe monolayer films and involved substrates. This provides a promising avenue via interface engineering for further increasing the T_c of monolayer FeSe and even other high-temperature superconductors in the future.

Acknowledgments. This work was financially supported by the National Natural Science Foundation of China (Grant No. 12141403), and the National Key R&D Program of China (Grant No. 2022YFA1403100).

References

[1] Wang Q Y, Li Z, Zhang W H, Zhang Z C, Zhang J S, Li W, Ding H, Ou Y B, Deng P, Chang K, Wen J, Song C L, He K, Jia J F, Ji S H, Wang Y Y, Wang L L, Chen X, Ma X C, and Xue Q K 2012 *Chin. Phys. Lett.* **29** 037402
[2] He S L, He J F, Zhang W H, Zhao L, Liu D, Liu X, Mou D X, Ou Y B, Wang Q Y, Li Z, Wang L, Peng Y Y, Liu Y, Chen C Y, Yu L, Liu G D, Dong X L, Zhang J, Chen C T, Xu Z Y, Chen X, Ma X C, Xue Q K, and Zhou X J 2013 *Nat. Mater.* **12** 605
[3] Zhang W H, Li Z, Li F S, Zhang H M, Peng J P, Tang C J, Wang Q Y, He K, Chen X, Wang L, Ma X C, and Xue Q K 2014 *Phys. Rev. B* **89** 060506(R)
[4] Pedersen A K, Ichinokura S, Tanaka T, Shimizu R, Hitosugi T, and Hirahara T 2020 *Phys. Rev. Lett.* **124** 227002
[5] Zhou Y J and Millis A J 2016 *Phys. Rev. B* **93** 224506
[6] Zhao W W, Li M, Chang C Z, Jiang J, Wu L, Liu C, Moodera J S, Zhu Y, and Chan M H W 2018 *Sci. Adv.* **4** eaao2682
[7] Song C L, Wang Y L, Jiang Y P, Z L, Wang L, He K, Chen X, Hoffman J E, Ma X C, and Xue Q K 2014 *Phys. Rev. Lett.* **112** 057002
[8] Zhang S Y, Wei T, Guan J Q, Zhu Q, Qin W, Wang W H, Zhang J D, Plummer E W, Zhu X, Zhang Z, and Guo J D 2019 *Phys. Rev. Lett.* **122** 066802
[9] Lee J J, Schmitt F T, Moore R G, Johnston S, Cui Y T, Li W, Yi M, Liu Z K, Hashimoto M, Zhang Y, Lu D H, Devereaux T P, Lee D H, and Shen Z X 2014 *Nature* **515** 245
[10] Zhang H M, Zhang D, Lu X W, Liu C, Zhou G Y, Ma X C, Wang L, Jiang P, Xue Q K, and Bao X H 2017 *Nat. Commun.* **8** 214
[11] Peng R, Zou K, Han M G, Albright S D, Hong H, Lau C, Xu H C, Zhu Y, Walker F J, and Ahn C H 2020 *Sci. Adv.* **6** eaay4517
[12] Zou K, Mandal S, Albright S D, Peng R, Pu Y, Kumah D, Lau C, Simon G H, Dagdeviren O E, He X, Boovi I, Schwarz U D, Altman E I, Feng D, Walker F J, Ismail-Beigi S, and Ahn C H 2016 *Phys. Rev. B* **93** 180506
[13] Tian Y C, Zhang W H, Li F S, Wu Y L, Wu Q, Sun F, Zhou G Y, Wang L, Ma X, Xue Q K, and Zhao J 2016 *Phys. Rev. Lett.* **116** 107001
[14] Song Q, Yu T L, Lou X, Xie B P, Xu H C, Wen C H P, Yao Q, Zhang S Y, Zhu X T, Guo J D, Peng R, and Feng D L 2019 *Nat. Commun.* **10** 758
[15] Peng R, Xu H C, Tan S Y, Cao H Y, Xia M, Shen X P, Huang Z C, Wen C H, Song Q, Zhang T, Xie B P, Gong X G, and Feng D L 2014 *Nat. Commun.* **5** 5044
[16] Pu Y J, Huang Z C, Xu H C, Xu D F, Song Q, Wen C H P, Peng R, and Feng D L 2016 *Phys. Rev. B* **94** 115146
[17] Ding H, Lv Y F, Zhao K, Wang W L, Wang L, Song C L, Chen X, Ma X C, and Xue Q K 2016 *Phys. Rev. Lett.* **117** 067001
[18] Rebec S N, Jia T, Zhang C, Hashimoto M, Lu D H, Moore R G, and Shen Z X 2017 *Phys. Rev. Lett.* **118** 067002
[19] Zhou G Y, Zhang Q H, Zheng F W, Zhang D, Liu C, Wang X X, Song C L, He K, Ma X C, L G, Zhang P, Wang L L, and Xue Q K 2018 *Sci. Bull.* **63** 747
[20] Song C L, Zhang H M, Zhong Y, Hu X P, Ji S H, Wang L, He K, Ma X C, and Xue Q K 2016 *Phys. Rev. Lett.* **116** 157001
[21] Tang C J, Zhang D, Zang Y Y, Liu C, Zhou G Y, Li Z, Zheng C, Hu X, Song C L, Ji S, He K, Chen X, Wang L, Ma X C, and Xue Q K 2015 *Phys. Rev. B* **92** 180507
[22] Koslowski B, Notz R, and Ziemann P 2002 *Surf. Sci.* **496** 153
[23] Yu X Q, Ren M Q, Zhang Y M, Fan J Q, Han S, Song C L, Ma X C, and Xue Q K 2020 *Phys. Rev. Mater.* **4** 051402(R)
[24] Bhat S G, Koshy A M, Pittala S, and Kumar P S A 2017 *AIP Conf. Proc.* **1859** 020007
[25] Song C L, Wang Y L, Cheng P, Jiang Y P, Li W, Zhang T, Li Z, He K, Wang L, Jia J F, Hung H H, Wu C J, Ma X C, Chen X, and Xue Q K 2011 *Science* **332** 1410
[26] Song Y H, Chen Z, Zhang Q H, Xu H C, Lou X, Chen X Y, Xu X F, Zhu X T, Tao R, Yu T L, Ru H, Wang Y H, Zhang T, Guo J D, Gu L, Xie Y W, Peng R, and Feng D L 2021 *Nat. Commun.* **12** 5926
[27] Barrett N, Rault J, Krug I, Vilquin B, Niu G, Gautier B, Albertini D, Lecoeur P, and Renault O 2010 *Surf. Interface Anal.* **42** 1690

[28] Xiong G, Shao R, Droubay T C, Joly A G, Beck K M, Chambers S A, and Hess W P 2007 *Adv. Funct. Mater.* **17** 2133
[29] Lim J Y, Oh J S, Ko B D, Cho J W, Kang S O, Cho G, Uhm H S, and Choi E H 2003 *J. Appl. Phys.* **94** 764
[30] Chalamala B R, Wei Y, Reuss R H, Aggarwal S, Gnade B E, Ramesh R, Bernhard J M, Sosa E D, and Golden D E 1999 *Appl. Phys. Lett.* **74** 1394
[31] Susaki T, Makishima A, and Hosono H 2011 *Phys. Rev. B* **83** 115435
[32] Zagonel L F, Büurer M, Bailly A, Renault O, Hoffmann M, Shih S J, Cockayne D, and Barrett N 2009 *J. Phys.: Condens. Matter* **21** 314013
[33] Zhou G Y, Zhang D, Liu C, Tang C J, Wang X X, Li Z, Song C L, Ji S H, He K, Wang L, Ma X C, and Xue Q K 2016 *Appl. Phys. Lett.* **108** 202603
[34] Zhang P, Peng X L, Qian T, Richard P, Shi X, Ma J Z, Fu B B, Guo Y L, Han Z Q, Wang S C, Wang L L, Xue Q K, Hu J P, Sun Y J, and Ding H 2016 *Phys. Rev. B* **94** 104510
[35] Zhang C F, Liu Z K, Chen Z Y, Xie Y W, He R H, Tang S, He J F, Li W, Jia T, Rebec S N, Ma E Y, Yan H, Hashimoto M, Lu D, Mo S K, Hikita Y, Moore R G, Hwang H Y, Lee D, and Shen Z 2017 *Nat. Commun.* **8** 14468
[36] Michaelson H B 1977 *J. Appl. Phys.* **48** 4729
[37] Song C L, Wang Y L, Jiang Y P, Li Z, Wang L, He K, Chen X, Ma X C, and Xue Q K 2011 *Phys. Rev. B* **84** 020503
[38] Mammadov S, Ristein J, Krone J, Raidel C, Wanke M, Wiesmann V, Speck F, and Seyller T 2017 *2D Mater.* **4** 015043
[39] Singh U R, Warmuth J, Markmann V, Wiebe J, and Wiesendanger R 2017 *J. Phys.: Condens. Matter* **29** 025004
[40] Edmonds M T, Hellerstedt J T, Tadich A, Schenk A, O'onnell K M, Tosado J, Butch N P, Syers P, Paglione J, and Fuhrer M S 2014 *ACS Nano* **8** 6400
[41] Kawasaki J K, Kim C H, Nelson J N, Crisp S, Zollner C J, Biegenwald E, Heron J T, Fennie C J, Schlom D G, and Shen K M 2018 *Phys. Rev. Lett.* **121** 176802
[42] Jia T, Chen Z, Rebec S N, Hashimoto M, Lu D, Devereaux T P, Lee D H, Moore R G, and Shen Z X 2021 *Adv. Sci.* **8** 2003454
[43] Stuckenholz S, Büchner C, Heyde M, and Freund H J 2015 *J. Phys. Chem. C* **119** 12283